

1 **Postmidnight equatorial plasma irregularities on June solstice during low solar activity**
2 **– a case study**

3

4 Claudia M. N. Candido^{1,2}, Jiankui Shi¹, Inez S. Batista², Fabio Becker-Guedes², Emília
5 Correia^{2,6}, Mangalathayil A. Abdu^{2,4}, Jonathan Makela³, Nanan Balan⁷, Narayan
6 Chapagain⁵, Chi Wang¹, Zhengkuan Liu¹

7

8 ¹National Space Science Center, NSSC, Chinese Academy of Sciences, State Key
9 Laboratory, China-Brazil Joint Laboratory for Space Weather, China

10 ²National Institute for Space Research – INPE, - São José dos Campos, SP, Brazil

11 ³Department of Electrical and Computer Engineering, University of Illinois at Urbana-
12 Champaign, Urbana, Illinois 61801, U.S.A

13 ⁴Instituto Tecnológico de Aeronáutica – ITA – São Jose dos Campos, Brazil

14

15 ⁵Departament of Physics, Patan Multiple Campus, Tribhuvan University, Latitpur, Nepal.

16

17 ⁶Centro de Radio Astronomia e Astrofísica Mackenzie, CRAAM, University Presbiteriana
18 Mackenzie – São Paulo – Brazil

19 ⁷Institute of Geology and Geophysics, Chinese Academy of Sciences, Beijing, China

20 Corresponding author: claudia.candido@inpe.br

21

22 *Keywords:* Solar minimum, Spread-F, Postmidnight plasma irregularities, equatorial
23 ionosphere, ionosonde, ionospheric forecast

24

25

26

27

28

29 **Abstract**

30

31 We present a case study of unusual spread-F structures observed by ionosondes at two
32 equatorial and low latitude Brazilian stations - Sao Luis (SL: 44.2° W, 2.33° S, dip angle:
33 -6.9°) and Fortaleza (FZ: 38.45°W, 3.9° S, dip angle: -16°). The irregularity structures
34 observed from midnight to post-midnight hours of moderate solar activity ($F_{10.7} < 97$ sfu,
35 where $1\text{sfu} = 10^{-22}\text{W.m}^{-2}.\text{s}^{-1}$) have characteristics different from typical post-sunset
36 equatorial spread-F. The spread-F traces first appeared at or above the F-layer peak and
37 gradually became well-formed mixed spread-F. They also appeared as plasma depletions in
38 the 630.0 nm airglow emissions made by a wide-angle imager located at nearby low latitude
39 station Cajazeiras (CZ: 38.56° W, 6.87° S, dip angle: -21.4°). The irregularities appeared
40 first over FZ and later over SL, giving evidence of an unusual westward propagation or a
41 horizontal plasma advection. The drift mode operation available in one of the ionosondes (a
42 Digital Portable Sounder, DPS-4) has enabled us to analyze the horizontal drift velocities
43 and directions of the irregularity movement. We also analyzed the neutral wind velocity
44 measured by a Fabry-Perot interferometer (FPI) installed at CZ and discussed its possible
45 role on the development of the irregularities.

46

47 **1 Introduction**

48

49 Equatorial spread-F representing small-scale to large-scale plasma irregularities has been
50 extensively studied for several decades. The large-scale plasma irregularities specifically
51 known as equatorial plasma bubbles (EPBs) are known to be associated with equatorial
52 spread-F. In the Brazilian equatorial sector, characterized by large negative magnetic
53 declination, spread-F and EPBs have high occurrence rates during local summer and
54 equinoctial months (Abdu et al., 1981a; Sahai et al., 2000; Sobral et al., 2002). However,

55 during low solar activity conditions, there is a class of spread-F/plasma irregularities
56 regularly observed in distinct longitudinal sectors, such as Brazil (Candido et al., 2011),
57 Africa (Yizengaw et al., 2013), and Asia (Nishioka et al., 2012). They are known as post-
58 midnight plasma irregularities (PMIs), which occur mostly in June solstice. Comprehensive
59 reviews on post-midnight plasma irregularities and plasma irregularities have been recently
60 published by Otsuka (2017) and Balan et al. (2018).

61 PMIs occur under conditions considered not favorable for the development of the Rayleigh-
62 Taylor (RT) instability, since that at night the vertical plasma drifts are downward, owing to
63 the westward electric fields. In recent years, a variety of works have reported their
64 occurrence both at low latitudes and equatorial region. Otsuka et al. (2009) and Nishioka et
65 al. (2012) investigated PMIs over Indonesia and discussed their possible sources. Li et al.
66 (2011) reported these irregularities observed over Hainan, China during low solar activity.
67 Candido et al. (2011) presented a study of PMIs observed over the south crest of the
68 equatorial ionization anomaly (EIA) during low solar activity, in CP, Brazil. Yokoyama et
69 al. (2011) studied unusual patterns of echoes from coherent scatter radar data occurring
70 around midnight during the solar minimum period. They observed two principal types of
71 irregularities: the upwelling plumes and MSTID-like striations. They have argued that the
72 former can be generated by both the RT instability (at equatorial region) or to Perkins
73 instability (at mid-latitude region) and the later only by the Perkins instability. Yizengaw et
74 al. (2013) presented the study of the PMIs over equatorial Africa, and also investigated their
75 most probable causes. Dao et al. (2016) reported in a very interesting work the occurrence of
76 postmidnight field-aligned irregularities (FAIs) in Indonesia during low solar activity in
77 2010.

78 Many instrumental techniques are currently providing high-quality measurements and
79 results for ionospheric studies. Early investigations of the ionosphere referred to the diffuse

80 echoes seen in data from measurements using ionosondes, which are high-frequency radars
81 used for ionospheric sounding (Breit and Tuve, 1926; Booker and Wells, 1938). The
82 “spread-F” is widely used to generically refer to the irregularities observed in the equatorial
83 and low-latitude regions. Nowadays, digital ionosondes are extensively used for ground-
84 based sounding of the ionosphere, providing information from the E-region to the peak of
85 the F-layer, over a variable range of frequencies as well as features related to the
86 propagation of the irregularities (Reinisch et al., 2004; Batista et al., 2008, Abdu et al.,
87 2009). Equatorial spread-F has been extensively studied for several decades, and it is known
88 to be associated with the occurrence of large-scale plasma irregularities or equatorial plasma
89 bubbles (EPBs).

90 Optical imaging of thermospheric emissions, like that used in this work, is also a useful
91 ground-based technique for studying thermosphere/ionosphere processes. All-sky imaging
92 systems provide images of thermospheric emissions (e.g., OI 630-nm, OI 777.4-nm
93 emissions) at ionospheric heights over a large horizontal extent. The OI 630-nm emission
94 comes from recombination processes between molecular oxygen and electrons and presents
95 a volumetric emission rate which peaks at an altitude of ~250 km, around the F-layer the
96 bottom side height. In this way, variations in the intensity of the emission (dark and bright
97 regions) are used as tracers of ionospheric irregularities, such as EPBs, or other
98 disturbances, such as travelling ionospheric disturbances - TIDs (Pimenta et al., 2008;
99 Abalde et al., 2009; Makela et al., 2010; Candido et al., 2011; Chapagain et al., 2012).

100 For clarity for the present study, which presents a distinct pattern of spread-F from those
101 usually observed in equatorial ionograms, we first address the current state of understanding
102 regarding spread-F signatures in ionosonde data.

103 It is currently accepted that there are two main spread-F types: range and frequency type
104 spread-F traces (Abdu et al., 1998). The range type spread-F, often associated with the

105 occurrence of medium and large-scale irregularities, including EPBs, is comprised of trace
106 patterns with the echoes spread in range and with the onset beginning at the lower frequency
107 end of the F-layer trace in ionograms. During the spread-F season in Brazil, between
108 October and March, the evening pre-reversal enhancement in the zonal electric field, and
109 therefore the F-layer vertical drift, attains large values and range type spread-F is observed
110 in equatorial ionograms, followed by their appearance at crest region of the EIA, which is
111 located around Cachoeira Paulista (CP: 22.4° S, 45° W, dip angle: -37°). During the
112 remaining part of the year, when the vertical drifts are very small (Batista et al., 1996),
113 spread-F is restricted to the height region below the F-layer peak, rarely reaching the topside
114 ionosphere, and therefore observed only close to the dip equator. This type of spread-F is
115 usually classified as bottom side spread-F (Valadares et al., 1983). The other common
116 spread-F pattern observed in equatorial ionograms is the frequency type spread-F. In this
117 case, the spread-F echoes are seen at frequencies around the F-layer critical frequency
118 (foF2). It is believed to be associated with smaller scale/decaying irregularities following
119 spread-F/EPBs (Abdu et al., 1981**b**).

120 Some studies have pointed out that frequency type spread-F can sometimes be associated
121 with patches of ionization propagating eastward (MacDougall et al., 1998). **However other**
122 **spread-F patterns are frequently observed in solstices in distinct longitudinal sectors as**
123 **reported in Brazilian (Candido et al., 2011, MacDougal et al., 2011), Asian (Yokohama et**
124 **al., 2011), African (Yinzengaw et al., 2013), and Peruvian (Zhan et al., 2018) sectors.** Also,
125 it is known that both frequency and range spread-F types can appear simultaneously, as a
126 mixed spread-F pattern. In this work, we present a case study on an unusual/anomalous
127 spread-F/plasma irregularities/depletions pattern observed over the equatorial region. We
128 use the term “unusual” in the sense that the observed features are distinct from those
129 typically observed for spread-F associated with post-sunset spread-F, as described above.

130 Although the unusual type of spread-F has been recognized since the early studies of the
131 equatorial ionosphere (Munro and Heisler, 1956; Heisler, 1958; Calvert and Cohen, 1961;
132 Bowman, 2001), this is the first time that it is reported for the Brazilian equatorial region
133 with simultaneous airglow observations, which reveal important ionospheric characteristics
134 not available when using only ionosonde data. The earlier studies extensively reported the
135 occurrence of anomalies in F-layer traces, such as cusps, F2 forking, and their possible
136 association with TIDs. Calvert and Cohen (1961) presented a comprehensive study of the
137 distinct spread-F patterns. They concluded that the distinct configurations or shapes of
138 spread-F were associated with the scattering in the vertical, east-west plane from field-
139 aligned irregularities and that the spread-F pattern depends on the position relative to the
140 ionosonde and the scale sizes of the irregularities.

141

142 **2. Data and Method**

143

144 **2.1 Digisondes**

145

146 We analyzed ionograms from two Digisondes DPS-4 operated at two Brazilian equatorial
147 sites: SL (44.2° W, 2.33° S, dip angle: -6.9°) and FZ (38.45° W, 3.9° S, dip angle: -16°),
148 which are separated in the east-west direction by ~ 600 km. Both instruments provided
149 ionograms at a 10-minute cadence. The DPS-4 also performs echo directional studies based
150 on Doppler interferometry, which provides information about the drift velocities associated
151 with irregularities. The operation of each Digisonde is based on the transmission of pulses at
152 digital frequencies from 1 to 20 MHz that are reflected from the ionosphere at plasma
153 frequencies lower than foF2. The maximum height range of the ionograms can be set at
154 ~ 700 or ~ 1400 km, for which the resolution is ~ 5 km and ~ 10 km, respectively. The

155 ionospheric true heights are calculated by an inversion method implemented by the ARTIST
156 software (Reinisch et al., 2005). Manual scaling of the data can be performed by editing the
157 ionograms using the SAO Explorer software (Galkin et al., 2008). The interferometry
158 system used by the Digisondes receiver is comprised of four small-spaced antennas for
159 signal reception arranged in a triangle with one antenna at the center. The signals from each
160 antenna are Fourier analyzed to identify echoes with different Doppler frequencies (for more
161 details see Reinisch et al., 2004). The Drift Explorer software determines the location of the
162 source regions of the spread-F echoes for each Doppler component. The ionograms present a
163 color code showing the direction of echoes that form the spread-F. The sky map and drift
164 data collected after the ionogram are derived from the measured Doppler frequency and
165 angle of arrival of reflected echoes. Special processing software enables us to plot skymaps
166 showing the location of all reflection sources. The Drift Explorer also provides plots of the
167 drift velocities (zonal, vertical, and meridional components). For more details about
168 Digisondes sounding modes and drift measurements see Reinisch et al. (2005) and
169 references therein.

170

171 **2.2 Wide-Angle Imaging System**

172 The airglow images of the OI 630-nm emission used in this study were measured by a
173 Portable Ionospheric Camera and Small-Scale Observatory (PICASSO) wide-angle imaging
174 system deployed at Cajazeiras (CZ: 6.87° S, 38.56° W, dip angle: -21.4°), located about
175 ~352 km from south of FZ. It is a miniaturized imaging system that measures the 630.0-nm
176 and 777.4-nm nightglow emissions. Since the 777.4-nm emission is generally very weak
177 during solar minimum conditions, we use only the 630.0-nm emission image data for this
178 study. The PICASSO images are captured on a 1024 × 1024 Andor DU434 CCD with a
179 spatial resolution of approximately 1 km (azimuthal) over the entire field of view. The

180 spatial resolution in the radial direction varies from ~1 km to ~5 km from zenith to the edge
181 of the field of view. The noise contributions from dark current are reduced by cooling the
182 CCD to at least -60°C. The exposure time for each image is 90 s, and dark images are taken
183 frequently to remove noise and read-out biases. For details about the data processing from a
184 similar PICASSO installation, see Makela and Miller (2008).

185

186 **2.3 Fabry-Perot Interferometer (FPI)**

187

188 FPIs are optical instruments that measure the spectral line shape of the 630.0 nm emission at
189 around 250 km of altitude and are very useful to study thermospheric winds from Doppler
190 shifts in the emission's frequency. For more details of the FPI technique, see Fisher et al
191 (2015) and references therein. The investigation of the departures of the background wind
192 system can be useful to explain possible sources of the F-uplifts associated with late-time
193 RT instability. For this purpose, we analyzed the behavior of the neutral winds over the
194 equatorial region taken from a ground-based FPI installed in CZ.

195

196 **3 Observations**

197

198 **3.1 Spread-F, F-layer height and plasma densities**

199

200 We present a case study of a spread-F event which occurred in the June solstice of 2011
201 during a geomagnetically quiet ($\Sigma Kp = 11$) night and low solar activity with mean F10.7 =
202 97 SFU (SFU is Solar Flux Unit = 10^{-22} W.m⁻².Hz⁻¹). Fig. 1 shows a sequence of ionograms
203 on 26 July 2011 from 00:40 LT to 03:10 LT over SL (top panel) and over FZ low-latitude
204 site (bottom panel) from 25 July 2011 at 22:00 LT to 26 July 2011 01:30 LT in which the

205 presence of unusual spread-F patterns is observed. Over SL, the first spread-F trace appears
206 at 01:00 LT at an oblique angle close to or above the F-layer peak at a virtual range of 600
207 km. Over the next hour, this structure gradually moves closer to the station SL, finally
208 merging with F-layer bottom side echoes and becoming a well-formed spread-F trace.
209 During the spread-F development, it is possible to observe an apparent small increase in the
210 F-layer heights. Finally, at the end of the spread-F event, around 02:50 LT, we observe a
211 decreased foF2 and the formation of an Es layer, lasting until 03:10 LT (not shown). We
212 notice a very similar evolutionary pattern of the structures in the FZ ionograms as in those
213 obtained from SL. However, the first spread-F traces appeared over FZ around 22:20 LT,
214 much earlier than over the equatorial site, SL. These echoes from FZ lasted for about 3
215 hours. The spread-F echoes gradually move closer to the station or downward to form a
216 well-structured spread-F pattern.

217 An important point to be considered is the local ionospheric background in which the
218 spread-F occurred. The F-layer parameters, $h'F$ (virtual height of the F-layer bottom side, in
219 km), the $hmF2$ (the real height of the F-layer peak, in km) and foF2 (the F-layer critical
220 frequency, in MHz) for both stations are shown in Fig. 2 from 18:00 LT to 06:00 LT. Over
221 SL an uplift of the F-layer was observed between 21:00 LT and 23:00 LT, not associated
222 with any spread-F echoes. Around 21:00 LT, at FZ, we may note some wave-like
223 oscillations in the F-layer height (notable in $hmF2$) with a period on the order of one hour.
224 The first spread-F trace at oblique angles (and perhaps above the F2 peak) appeared just
225 after these oscillations, as shown by the blue lines connecting the $h'F$ and $hmF2$ curves.

226 On the other hand, over FZ where heights are lower, we observe stronger wave-like
227 oscillations in both $h'F$ and $hmF2$ three hours earlier than observed at SL. The F-layer
228 critical frequency decreased for both stations, as it is expected for this period. At the
229 beginning of the spread-F occurrence, the foF2 was as low as 4 MHz, corresponding to an

230 electron density of 1.98×10^5 el.cm⁻³. The parameter fxI (not shown), or top frequency of
231 spread-F, which is the highest frequency of spread-F echoes, reached values not higher than
232 4.5 MHz over SL but reached values around 6.0 MHz over FZ, which means higher plasma
233 density at this region. Moreover, after the spread-F ceased, it was possible to observe the
234 recovery of the plasma frequency/density over FZ sooner than over SL, as shown in the both
235 panels around 05:30 LT.

236

237 3.2 Depletions in the airglow OI 630.0-nm emission

238

239 Figure 3 shows a sequence of four images of the OI 630.0-nm emission collected on 25-26
240 July 2011 at Cajazeiras (CZ: center of the frame), Brazil. The images are projected over a
241 geographic map of Brazil assuming an emission altitude of 250 km. The sites of FZ and SL
242 are also indicated in the top-left panel. Between 23:12 LT to 01:26 LT at least two
243 depletions (dark regions passing over FZ and CZ) can be observed propagating westward.
244 These depletions propagated over FZ and CZ at 23:12 LT, in agreement with the spread-F
245 traces seen in the ionograms from FZ.

246

247 3.3 F-layer irregularity Drifts – Directions and Velocities

248 Automatic drift mode routines were used to obtain information about the location of echo
249 sources in the F-layer associated with plasma irregularities. These routines provide
250 information about the distance of the reflected echoes, using measurements of the radar
251 ranges to the vertical and oblique echoes as well as their directions, as described by Reinisch
252 et al. (2004). The distribution of the echoes can be displayed in skymaps as shown in Fig. 4.
253 Skymaps between 00:12 LT and 00:42 LT were constructed using data from FZ during the
254 spread-F event studied where reflected echoes appear and are distributed in a west-east

255 elongated pattern covering a total horizontal distance of 1200 km (from west to east). It may
256 be noted that, in general, negative Doppler velocity (yellow color) of the echoes dominates
257 the western azimuth while the eastern azimuth is dominated by positive Doppler velocity
258 (blue color), a characteristic that is indicative of an overall westward motion of the
259 irregularity structures. Additional directional information is obtained from the temporal
260 evolution of each spread-F echo in plots of the horizontal distance of the echoes (horizontal
261 axis) as a function of time (vertical axis), presented as directograms. A directogram for the
262 night of 25-26 July 2011 constructed using data from FZ is shown in Fig. 5. Each horizontal
263 line of the directogram corresponds to a single ionogram. The spread echoes are distributed
264 east to west mainly from 23:00 LT to ~ 01:00 LT, although there is only a sparse distribution
265 between 21:00 and 23:00 LT. The color codes at both sides indicate the location (at east or
266 west) and the incoming and outgoing direction (arrows) of the reflectors (irregularities), for
267 example, the first echoes are seen at the zonal distance of ~320 km between 23:00 and 23:30
268 LT coming from East (red squares). The color code indicates they are at east of the station
269 coming from the east side. Also, there are echoes at the east of the station which come from
270 northeast, NNE, direction. Among these echoes, there are only a few points that are going
271 eastward (blue points). From 23:30 to 01:30 LT, there are echoes at west which gradually
272 disappear after 02:00 LT. The color code to the left shows that they are at west from the
273 station and going westward. Thus, the echoes present a mean westward propagation. We
274 point out that the horizontal distance range limit is around 600 km, which correspond to an
275 antenna beam angle of approximately 45° , as it is seen in the directograms on Fig. 5, and
276 h_{min} is the spread-F reflection height.

277 The unusual spread-F echoes were observed at both equatorial sites, SL and FZ, with a zonal
278 separation of ~600 km. The first spread-F trace was observed at 22:20 LT over FZ and later
279 at 01:00 LT over SL. This lag of ~ 02:40 hours suggests an average westward drift velocity

280 component of $\sim 62 \text{ ms}^{-1}$. The DPS-4 drift mode provides the full-vector Doppler velocity for
281 the observed echoes. Figure 6 shows the variation of the V_z (vertical component) and V_{east}
282 (zonal component) velocities taken from measurements of the Digisonde DPS-4 (drift mode)
283 from 21:00 LT on July 25, 2011, to 04:00 LT on July 26, 2011. Positive (negative) V_{east}
284 velocities represent eastward (westward) propagation. $|V|$ represents the zonal drift Doppler
285 velocities ($<60 \text{ ms}^{-1}$), while the maximum vertical upward component is $\sim 30 \text{ ms}^{-1}$. The zonal
286 velocities inferred from Drift Explorer agree well with the estimate obtained from the
287 difference in onset times of spread-F echoes between SL and FZ, with a mean value of ~ 55
288 ms^{-1} during the event. The middle panel is the vector diagram with the variations of the
289 mean total electrodynamical drift velocity (see Balan et al., 1992). For clarity, the vector
290 length is fixed, and the information on $|V|$ is represented by the concentric circles (arrow
291 start point). As it is observed, the vector is found to rotate anticlockwise, starting in the east-
292 up sector in the night and reaching west-up sector in post-midnight. Velocities extracted
293 from the airglow images obtained from CZ are shown in the bottom panel of Fig. 6. To
294 estimate the velocity of the depletion structure, the individual images were processed by first
295 spatially registering the 630.0-nm images using the star field. After removing the stars from
296 the images using a point suppression methodology, the images were projected onto
297 geographic coordinates assuming an airglow emission altitude of 250 km (for details of
298 analysis technique see Chapagain et al., 2012). The depletion structure was selected in
299 consecutive images to find the zonal shift of the structures from which the velocity was
300 estimated. The estimated zonal propagation velocity was $\sim 60 \text{ ms}^{-1}$, which agrees well with
301 the velocities determined by the Doppler technique of the Digisonde. We should keep in
302 mind that the Digisonde Doppler technique determines the mean irregularity motion while
303 the velocities from the airglow technique estimate the mean propagation of the plasma
304 depletion.

305 Besides the capabilities of the Digisonde to sound and detect the occurrence of plasma
306 irregularities seen in the ionograms as spread-F echoes, and the F-region heights variations,
307 and their vertical drifts, there is a method which uses the true heights to obtain information
308 about the gravity waves oscillations at specific plasma frequencies. The true heights are
309 extracted from virtual heights by an inversion algorithm used in the SAO Explore software.
310 This method was described in detail by Abdu et al., 2009, in a comprehensive study about
311 the influence of gravity waves on the equatorial spread-F. In their work, the same both
312 locations were analyzed: the off-equator station FZ and the equatorial station SL. Because of
313 the both stations is more separated in longitude than in latitude, it was assumed that GW
314 oscillations present in the bottomside F-layer FZ could have the same features at SL,
315 considering few differences attributed to the inclination magnetic field in each one. In this
316 work, we also took advantage of the simultaneous Digisonde sounding at these stations in
317 order to verify the possible influence of GW as precursor of the instability growth which
318 leads to late development of spread-F studied.

319 Figure 7 presents the oscillations in F-layer true height at fixed frequencies (1.5-5.0
320 MHz) in both stations, SL and FZ. It is possible to observe oscillations prior the
321 development of spread-F especially in FZ, with periods around 1 hour, which will be
322 discussed later in session 4.3.4

323

324 **3.4 Thermospheric Winds**

325 Figure 8 shows the measured thermospheric zonal (top panel) and meridional (bottom panel)
326 wind on July 25-26, taken from the FPI installed in CZ, the same location where the airglow
327 images were obtained. The shaded region encloses the standard deviation of the monthly
328 average, the green lines are the average winds on July 25-26 (± 2 days), and the red line is the
329 measurement for July 25-26. It is observed that on July 25-26 between 22:00 LT and 01:00

330 LT the zonal wind is abnormally eastward (~100 m/s), while the meridional wind departs
331 from the monthly and daily variation average. From this, we can consider that a possible
332 balance between the zonal and meridional wind component may be responsible by plasma
333 advection (plasma movement) from low-latitude to equatorial region, which might have
334 maintained the F-layer at a higher altitude as discussed by Nicolls et al., 2006. This apparent
335 uplifts observed in both stations around 00:00 LT might have caused the growth of the late
336 RT-instability and the PMIs.

337

338 **4 Discussion**

339

340 We present an unusual event of PMIs/spread-F/depletions over the equatorial site in Brazil
341 that exhibits singular features. This is the first report of such distinct pattern of spread-F for
342 the Brazilian equatorial region, though it was observed earlier at the low-latitude station CP
343 (Brazil) for the solar minimum 2008-2009 by Candido et al., 2011. **By distinct we mean that**
344 **they occur in postmidnight hours, propagating westward, which is not usually observed**
345 **during solar minimum unless there are a previous eastward EPB structure propagation, as**
346 **mentioned by Paulino et al., 2010.** A careful analysis of equatorial ionograms and other plots
347 from digisonde soundings suggest modifications in the ionospheric plasma density
348 structuring, such as those associated with plasma density depletions, which are responsible
349 for a variety of spread F-layer patterns.

350

351 **4.1 Depletions in the airglow OI 630.0 nm images**

352

353 Airglow images show an apparent southwestward propagation of depletions on this night,
354 which differs from the typical propagation direction of post-sunset EPBs. However, this

355 atypical propagation can be a characteristic of post-midnight depletions and needs further
356 investigation with a long-term airglow database. The depletions also propagated over CZ
357 (350 km south of FZ) with mean westward velocities $\sim 60 \text{ ms}^{-1}$ which are similar to the
358 velocities of propagation of the irregularities observed with the Digisonde at FZ. Some
359 authors have demonstrated that EPBs can also present westward propagation after midnight
360 during quiet times (Paulino et al., 2010; Sobral et al., 2011). However, they defined in those
361 studies that the depletions associated with EPBs should first present movement to the east
362 earlier in the evening and reversal to westward at later hours. This is not the case for the
363 structures presented in this work since there are no depletions in the OI 630.0-nm images
364 propagating eastward earlier in the evening.

365 Moreover, Sobral et al. (2011), interpreted that westward traveling plasma bubbles (WTPB)
366 observed at the same region were associated with westward zonal thermospheric winds
367 (simulated results). On the other hand, Fisher et al. (2015) presented a climatological study
368 of the quiet time thermospheric winds and temperatures by measurements of the OI 630.0
369 nm airglow emission spectral line shape over the same region. They noticed that during low
370 solar activity ($F_{10.7} < 125 \text{ sfu}$), the zonal and meridional winds are, on average, negligible
371 in postmidnight hours. It is possible that these differences can be attributed to departures
372 from the wind system at which could be responsible by the F-layer uplifts and plasma
373 instabilities/irregularities development.

374

375 **4.2 Spread-F in ionograms**

376 As mentioned before, spread-F echoes in ionograms generally appear first at the low-
377 frequency end, as satellite traces, evolving into spread-F echoes extended in frequency and
378 range. These characteristics were not seen in the present study. In this work, the reflected
379 echoes observed in the ionograms first came from oblique directions and at heights which

380 could be considered possibly higher than those observed overhead. The spread echoes
381 appear at the higher frequency edge of the F-layer, with top-frequency higher than the layer
382 critical frequency. Subsequently, the low-frequency edge of the cusp merges with the main
383 trace, while the baseline of the spread-F traces gradually decreases in height. Anomalous
384 traces in F-layer ionograms, such as ‘cusps’ or ‘spurs,’ were described in earlier studies to
385 be associated with traveling disturbances in the ionosphere. Munro and Heisler (1956) and
386 Heisler (1958) have observed the occurrence of anomalous traces in ionograms and
387 attributed them to the manifestations of TIDs. As it is well known, TIDs can be described as
388 frontal gravity waves propagating horizontally in the ionosphere, causing increases and
389 decreases in the ionization, i.e., horizontal gradients in the ionization. According to Munro
390 and Heisler (1956), changes in the ionization would be responsible for the anomalous traces
391 in the F-layer ionogram. Similar occurrences were reported by Ratcliffe (1956) for
392 ionograms from Huancayo, Peru. Calvert and Cohen (1961) have pointed out that some
393 spread-F traces observed over Huancayo presented characteristics similar to frequency
394 spread-F from “temperate” latitudes, which are mainly associated with TIDs. Also, they
395 studied distinct configurations of spread-F with echoes coming from oblique directions,
396 similar to what is presented in this work. The oblique echoes observed in ionograms alone
397 could not provide their zonal direction (from east or west). However, additional directional
398 information provided from the drift mode sounding of the Digisonde DPS-4 and their
399 appearance first in the ionograms over FZ followed by their occurrence over SL (a western
400 site in relation to FZ), suggested that they propagated westward. Late/pre-dawn spread-F
401 was also reported by McDougall et al. (1998) for solstices in the Brazilian sector. However,
402 they considered the occurrence of late time spread-F during December solstice at Fortaleza
403 as patches of ionization, which cause spread echoes at the high-frequency end or the

404 frequency spread-F. They also concluded that the echoes did not come from overhead
405 structures but from the east or west directions.

406

407 **4.3 Post-midnight irregularities/F-region background conditions**

408

409 As it is well-known, the poor alignment between the sunset terminator and the magnetic
410 field lines during June solstice in Brazil is responsible by the low occurrence rate of post-
411 sunset spread-F/EPBs, since the vertical plasma drifts are very weak. However, it is
412 observed a occurrence peak of late night spread-F/plasma irregularities in June solstice,
413 especially around midnight and post-midnight. For this, it is necessary to have an F-layer
414 uplift, which creates favorable conditions for the development of the RT instability. These
415 conditions are not completely understood, and they have been discussed by several authors
416 (McDougall et al., 1998; Nicolls et al., 2006; Abdu et al., 2009; Nishioka et al., 2012,
417 Yokohama et al., 2011, Ajith et al., 2016).

418 During the high solar activity, the longitudinal variation of the declination angle is
419 predominant on the F-layer vertical drift and the occurrence of the plasma irregularities,
420 while it is not important during solar minimum. During low solar activity/solar minimum, in
421 the absence of geomagnetic disturbances, the seeding processes related to gravity waves
422 seem to be more important, especially when the PRE-amplitude is small or absent
423 (Balachandran et al., 1992; Abdu et al., 2009). In this way, we should address the conditions
424 which precede the occurrence of the post-midnight irregularities observed in this work. It is
425 noticed that spread-F traces associated with plasma irregularities were detected firstly at
426 oblique directions at least 500 km at east or west from the station, as seen in the
427 directograms in Figure 5, which we can consider as ionospheric conditions favorable in a
428 wide longitudinal range.

429 **4.3.1 Thermospheric winds**

430

431 Nicolls et al. (2006) discussed the nocturnal F-layer uplifts associated with the secondary
432 maximum of spread-F occurrence rate in low solar activity. As it is well understood, the
433 nocturnal westward electric field is responsible by the downward movement of the F-layer.
434 During solar minimum, these electric fields can be easily reversed by a weak geomagnetic
435 disturbance. However, in the absence of the geomagnetic disturbance, which is the case
436 studied in this work, other sources should be considered. Analyzing F-layer uplifts for
437 different conditions of solar activity, Nicolls et al. (2006) verified that during downward F-
438 layer movement (decreasing westward electric field), even a small contribution of a
439 meridional equatorward wind (~ 30 m/s), could lead the F-layer to higher heights triggering
440 the RT instability.

441 Moreover, it was discussed that neutral winds could not uplift the equatorial plasma directly,
442 but they are sources of meridional advection (movement) of plasma, driven by a latitudinal
443 gradient in electron density, responsible by F-layer uplifts. They concluded that the uplifts
444 could be due to the decreasing, not to the reversal, of the westward zonal electric field
445 associated with departures in the wind system related to the midnight temperature maximum
446 (MTM), recombination processes, and the plasma flux. In this way, we analyze the zonal
447 and the meridional neutral wind variation in Figure 8, in order to verify that there are
448 suitable conditions for F-layer uplift. As it is observed in Figure 8 (top panel), the zonal
449 wind is ~ 100 m/s just before midnight while meridional wind (equatorward) is ~ 30 m/s just
450 after midnight (bottom panel). There is evidence that the mean equatorward meridional
451 winds have kept the F-layer at higher altitudes enough to the trigger the RT instability
452 development.

453

454 4.3.2 Recombination processes - Rayleigh Taylor instability growth rate

455 Nishioka et al. (2012) discussed the causes of the postmidnight uplifts that occurred during
456 winter in Chumphon, Thailand (low latitude) and the post-midnight Field-Aligned
457 Irregularities, FAIs, in Kototaband, Indonesia (equatorial region). As it is well known, the
458 zonal electric field is westward during the night, as the vertical drift $\mathbf{E} \times \mathbf{B}$ is downward. This
459 condition leads to a negative RT-instability growth rate. In this way, it is important to
460 address, the importance of the term g/v_{in} in the linear growth rate of RT-instability, and of
461 the recombination processes, as shown in Equation (1):

$$462 \quad \gamma = \left(\frac{E}{B} + \frac{g}{v_{in}} \right) \frac{1}{L} \quad (1)$$

463 Where: E is an the electric field; B is the magnetic field; g is gravity acceleration, v_{in} is ion-
464 neutral collision frequency; L is the scale length of the vertical gradient of the F-region
465 plasma density. At night, the zonal electric field is westward, as the growth rate can be
466 negative, i.e., the F-layer bottom side is stable. On the other hand, the term g/v_{in} may
467 increase in the following conditions: 1) v_{in} is proportional to the neutral density, n , where n
468 is smaller during the night than the day; 2) v_{in} is smaller at higher altitudes owing to the
469 decrease of n with the height; 3) v_{in} is smaller during low solar activities. Therefore, under
470 the appropriate conditions, the RT growth rate can be positive, although small, as it is
471 observed in this work. To understand the recombination processes as a source of the F-layer
472 uplift it should be considered that the F-layer bottom side is eroded if it is at lower altitudes
473 (at ~300 km), such as there is a decreasing of peak density and the increasing of F-layer
474 peak height. For clarity, we present the F-layer density profiles, in Fig. 9, taken from
475 measurements using the Digisonde installed in SL. It is possible to observe that from 22:00
476 to 00:00 LT, the F-layer peak height, and peak density decrease. As the F-layer bottom side

477 is at a lower height, it is observed an apparent F-layer uplift, which can be attributed to the
478 recombination process at the bottom side.

479

480 **4.3.3 Es-layer electric fields**

481

482 The role of Es-layer has been considered as a possible cause for the late-time RT instability
483 development. **Low-latitude** Es-layer can provide enough polarization electric field which
484 maps to equatorial F-layer bottom side, causing F-layer uplift, as pointed out by Yizengaw
485 et al. (2013). They interpreted the occurrence of late plasma irregularities/EPBs over Africa
486 coast during the same period of this work, June solstice 2011, and discussed that during
487 quiet geomagnetic nights, there were favorable conditions for the action of polarization
488 electric fields associated with **low-latitude** Es-layer/instability which mapped to the
489 equatorial F-layer along the geomagnetic field lines seeding RT-instability and irregularities.
490 In fact, in this work, we can observe the occurrence of the Es-layer at the both quasi-
491 equatorial station FZ and at SL, at around 00:00 and 02:50 LT respectively. However, the
492 influence of Es-layers on late time F-layer uplift in this work is not clear since they occur at
493 the same location of the spread-F. Its influence on the post-midnight spread-F during solar
494 minimum is worth of investigation in further works.

495

496 **4.3.4 Mesoscale Travelling Ionospheric Disturbances, MSTIDs and Gravity-Waves,** 497 **GW**

498 MSTIDs have been reported in Brazilian low latitudes using airglow and ionosonde
499 (Candido et al., 2008, 2011; Pimenta et al., 2008). They appear as large-scale dark bands
500 aligned from northeast to southwest propagating northwestward mainly during low solar
501 activity and are associated with electrodynamic forces in mid-latitudes (Perkins instability)

502 or by the propagation of gravity waves in ionospheric heights at low latitudes or equatorial
503 region. If they propagate at equatorial ionospheric heights, they can be seen as oscillations in
504 the F-layer bottom side and can trigger RT-instability and plasma bubbles. In this work, the
505 plasma irregularities seen by the ionosonde are preceded by small oscillations in the F-layer
506 bottom ($h'F$) and peak heights ($hmF2$). However, oscillations are usually observed in the F-
507 layer bottom side, and it should be carefully considered in order to establish if they are
508 associated with GWs. Generally, they are considered associated with GW if it downward
509 phase propagation is observed in the fixed frequencies (isolines) plots, i.e., the oscillations
510 are seen firstly in the higher frequencies. Figure 7 showed the occurrence of oscillations in
511 F-layer through some fixed frequencies (isolines) in both stations FZ and SL, although the
512 downward propagation is not exactly clear. On the other hand, the spread-F pattern observed
513 in this work is quite similar to those reported by Candido et al. (2011) during the descending
514 phase/solar minimum at low latitudes in CP. This feature could suggest that they could be
515 caused by low latitudes MSTIDs propagating equatorward or associated to the action of
516 polarization electric fields mapping from low latitudes MSTIDs structures to the equatorial
517 F-layer bottom side. This kind of event was reported by Miller et al. (2009), which studied
518 the occurrence of EPBs on the same night of the occurrence of MSTIDs propagating in mid-
519 latitudes and attributed them to the action of the electric field from these MSTIDs in the F-
520 layer region. However, the depletions observed in the OI 630-nm emission (Figure 3)
521 present distinct features (propagation direction) of those associated to MSTIDs coming from
522 low latitudes reported by Candido et al. (2011). Also, they are not similar to the depletions
523 associated with the typical EPBs which propagate eastward. Recent results by Takahashi et
524 al. (2018) reported the occurrence of equatorial MSTIDs in high solar activity conditions
525 (2014/15), which were associated with periodic plasma bubbles in the Total Electron

526 Content (TEC) maps in the same region. They showed evidence of tropospheric sources for
527 the development and propagation of GWs at ionospheric heights.

528 Finally, we should address that, as shown in Figs.2 and 7, late height rise (in both $h'F$ and
529 $hmF2$) with smaller amplitude waves are observed at SL starting at $\sim 21:00$ LT when the
530 base height ($h'F$) increased to > 250 km. Such a condition can be suitable for the growth of
531 RT instability. Over FZ, a similar sequence of variations occurred starting at $\sim 23:00$ LT in
532 $hmF2$. Notice that $h'F$ and $hmF2$ values were significantly smaller than those at SL.
533 However, it is notable that the oscillations in the F layer heights, especially in $hmF2$, (with
534 the period around 36 min) that preceded the spread F traces (at both sites) are significantly
535 higher in amplitude at FZ than at SL. This aspect can be noted in more detail in the iso-line
536 plots of plasma frequencies presented in Fig. 7, where in the height oscillations show larger
537 amplitude and occurring at earlier local times than they are at SL. Such oscillations may be
538 associated with gravity waves propagating to ionospheric heights with preferential
539 propagating directions to northeast and southeast, as recently reported by Paulino et al.
540 (2016). These oscillations are indicative of the seed perturbations to lead to the SF
541 irregularity development through RT mechanism. Depending upon the amplitude of the seed
542 perturbation, even the small increases in the F layer height that marked this period, could be
543 capable of seeding RT instability and consequently generate the spread F irregularities (see,
544 for example, Abdu et al., 2009). To explain the non-local origin of the SF traces, as observed
545 at both sites, it will be necessary to assume that the precursor conditions that existed at SL
546 and FZ must have continued to exist in longitude extending further eastward of Fortaleza,
547 perhaps with some increase in intensity so that the irregularities generated therein and
548 drifting westward could be the origin of the oblique spread F trace first observed over FZ
549 and later over SL.

550 It is plausible to consider that the depletions observed in this work can be associated with
551 atypical EPBs triggered by GWs/MSTIDs at locations at the east of FZ and SL or to F-layer
552 uplifts caused by departures from wind system simultaneously to a weakening of the
553 westward zonal electric field (not shown here) during low solar activity. We should notice
554 that the observational techniques used in this work are complementary and validate each
555 other to identify “anomalous” spread-F patterns associated with plasma
556 irregularities/depletions and can help the understanding of the ionosphere during low solar
557 activity. The drift mode is very useful and suitable for tracking plasma irregularities and
558 their evolution in the absence of other techniques.

559

560 **5 Summary and Conclusions**

561 In this paper, we have presented and discussed an unusual spread-F pattern associated with
562 unusual depletions on the OI 630.nm airglow emission observed during geomagnetically
563 quiet conditions during the June solstice of 2011 over the equatorial region in Brazil. We
564 summarize our findings as:

565 1) The unusual spread-F pattern studied in this work present a distinct feature from those
566 usually observed at post-sunset hours, with spread-F appearing firstly at the higher
567 frequency edge of the F-layer trace and evolving to a mixed (frequency and range) spread-
568 F;

569 2) The spread-F/depletions occurred during low plasma density conditions, geomagnetically
570 quiet nights, low solar activity and propagated westward. For the studied case, there no
571 evidence of previous depletions propagating eastward.

572 3) The processes to generate spread-F at equatorial latitudes during quiet time seems to be
573 associated with the late time F-layer uplifts, possibly caused by departures in the neutral
574 wind system. On its turn, departures in the neutral wind system may be caused by an

575 increased auroral activity, which in this present study may be associated to the occurrence of
576 a short-duration event of high speed stream (this possible influence is the subject of an
577 ongoing study). Moreover, departures of the wind system associated to a weakening of the
578 westward electric field, or to the propagation of GWs at ionospheric heights, favor the
579 development of the late-time RT-instability. Further studies enclosing simulations are in
580 progress.

581 4) The spread-F event discussed here presents characteristics similar to those of the earlier
582 cases reported for low latitudes in CP (around the south crest of the EIA), during June
583 solstice of solar minimum 2008-2009 by Candido et al., 2011 and interpreted as the
584 signature of the passage of mid-latitude MSTIDs in the ionograms.

585 5) The instrumental approach in this work seems to be suitable for further ionospheric
586 studies, modeling, and forecast during low solar activity.

587

588 **Abbreviations**

589

590 SL: Sao Luis

591 FZ: Fortaleza

592 CZ: Cajazeira

593 CP: Cachoeira Paulista

594 DPS: Digital portable sounder

595 FPI: Fabry-Perot Interferometer

596 EPBs: Equatorial plasma bubbles

597 PMIs: Postmidnight plasma irregularities

598 RT: Rayleigh-Taylor

599 EIA: Equatorial ionization anomaly

600 MSTIDs: Meso-scale traveling ionospheric disturbances

601 FAIs: Field-aligned irregularities
602 TIDs: Travelling ionospheric disturbances
603 SFU: solar flux unity
604 LT: local time
605 UT: Universal time
606 MTM: midnight temperature maximum
607 GWs: Gravity waves

608

609 **Data availability**

610 The processed data used in this work can be requested to the author CMNC by the email:
611 claudia.candido@inpe.br. The authors thank to the Embrace/INPE Program for the
612 Digisonde raw data which can be downloaded from the website: www.inpe.br/embrace. The
613 airglow and Fabry-Perot data should be requested to the author: JM, by the email:
614 jmakela@illinois.edu.

615

616 **Author Contributions**

617 CMNC wrote the manuscript and plotted the graphics of the ionospheric parameters. FBG
618 helped with part of the graphics and revised the manuscript. JS, ISB, EC, MAA, N.B., ZL,
619 CW read and made suggestions to the manuscript. JM and NC provided the airglow figures
620 and Fabry-Perot data and plots, as well as read the manuscript and suggested corrections. All
621 the authors read, give comments and suggestions to the work and agree with the content and
622 submission of this manuscript.

623

624 **Competing interests**

625 The authors declare they have no conflicts of interest.

626

627 **Acknowledgments**

628 C.M.N.C thanks the Brazilian funding agency CNPq for the financial support through the
629 process n.64537/2015-5, to China-Brazil Joint Laboratory for Space Weather for the
630 postdoctoral fellowship. J. Shi thanks the National Natural Science Foundation of China for
631 the project No. 41674145. Also, the authors thank to the Program
632 EMBRACE/INPE/MCTIC for providing ionospheric data to this work. N.P.C. was
633 supported by the NASA Living With a Star Heliophysics Postdoctoral Fellowship Program,
634 administered by the University Corporation for Atmospheric Research (UCAR). Work at the
635 University of Illinois at Urbana-Champaign was supported by National Science Foundation
636 CEDAR grant AGS 09-40253 and was performed in collaboration with J. W. Meriwether at
637 Clemson University. We are grateful to the Universidade Federal de Campina Grande and
638 Dr. Ricardo A. Buriti for the support to the imaging systems installed at Cajazeiras.

639

640 **6 References**

641

642 Abalde, J. R., Sahai, Y., Fagundes, P. R., Becker-Guedes, F., Bittencourt, J. A. , Pillat, V.
643 G., Lima, W. L. C., Candido, C. M. N., de Freitas, T. F., Day-to-day variability in the
644 development of plasma bubbles associated with geomagnetic disturbances, J. Geophys. Res.,
645 114, A04304, doi:10.1029/2008JA013788, 2009.

646

647 Abdu, M. A., Bittencourt, J. A., Batista, I. S., Magnetic declination control of the equatorial
648 F region dynamo field development and spread F, J. Geophys., Res., v. 86, p. 11443-11446,
649 1981a.

650

651 Abdu, M. A., Batista, I. S., Bittencourt, J. A., Some characteristics of spread F at the
652 magnetic equatorial station Fortaleza, *J. Geophys. Res.*, 86, A8, 6836-6842, 1981b.

653

654 Abdu, M. A., Sobral, J. H. A., Batista, I. S., Rios, V. H., Medina, C., Equatorial spread F
655 occurrence statistics in the American longitudes: Diurnal, seasonal and solar cycle
656 variations, *Adv. Space Res.*, 22(6), 851–854, 1998.

657

658 Abdu, M. A., Batista, I. S., Reinisch, B. W., de Souza, J. R., Sobral, J. H. A., Pedersen, T.
659 R., Medeiros, A. F., Schuch, N. J., de Paula, E. R., Groves, K. M., Conjugate Point
660 Equatorial Experiment (COPEX) campaign in Brazil: Electrodynamics highlights on spread
661 F development conditions and day-to-day variability, *J. Geophys. Res.*, 114, A04308,
662 doi:10.1029/2008JA013749, 2009.

663

664 Ajith, K. K., Tulasi Ram, S., Yamamoto, M., Otsuka, Y., Niranjana, K., On the fresh
665 development of equatorial plasma bubbles around the midnight hours of June solstice, *J.*
666 *Geophys. Res. Space Physics*, 121, 9051–9062, doi:10.1002/2016JA023024, 2016.

667

668

669 Balachandran Nair, R., Balan, N., Bailey, G. J., Rao, P. B., Spectra of the ac electric fields in
670 the post-sunset F-region at the magnetic equator, *Planet. Space Sci.*, 40(5), 655–662.
671 [https://doi.org/10.1016/0032-0633\(92\)90006-A](https://doi.org/10.1016/0032-0633(92)90006-A), 1992.

672

673 Balan, N., Jayachandran, B., Balachandran Nair, R., Namboothiri, S. P., Bailey, G. J., Rao,
674 P. B., HF Doppler observations of vector plasma drifts in the evening F-region at the
675 magnetic equator, *J. Atmos. Terr. Phys*, 54, (11/12), pp. 1545-1554, 1992.

676

677 Balan N., Liu, L. B., Le, H. J., A brief review of equatorial ionization anomaly and
678 ionospheric irregularities, *Earth Planet. Phys.*, 2(4), 1–19.
679 <http://doi.org/10.26464/epp2018025>, 2018.

680

681 Batista, I. S., de Medeiros, R. T., Abdu, M. A., de Souza, J. R., Equatorial Ionospheric
682 Vertical Plasma Drift Model over the Brazilian Region, *J. Geophys. Res.*, 101 (A5), 10887-
683 10892, 1996, 1996.

684

685 Batista, I. S., Abdu, M. A, Ionospheric variability at Brazilian low and equatorial latitudes:
686 Comparison between observations and IRI model, *Adv. Space Res.*, 34, 1894–1900,
687 doi:10.1016/j.asr.2004.04.012, 2004.

688

689 Batista, I. S., Abdu, M. A., Carrasco, A. J., Reinisch, B. W., Paula, E. R., Schuch, N. J.,
690 Bertoni, F., Equatorial spread F and sporadic E-layer connections during the Brazilian
691 Conjugate Point Equatorial Experiment (COPEX), *J. Atmos. Sol. Terr. Phys.*, 70, 1133-1143,
692 doi:10.1016/j.jastp.2008.01.007, 2008.

693

694 Booker, H. G., Wells, H. W., Scattering of radio waves in the F-region of the ionosphere,
695 *Terr. Magn. Atmos. Electr.*, 43, 249–256, doi:10.1029/TE043i003p00249, 1938.

696

697 Bowman, G. G., A comparison of nighttime TID characteristics between equatorial
698 ionospheric anomaly crest and midlatitude regions, related to Spread F occurrence, *J.*
699 *Geophys. Res.*, 106(A2), 1761–1769, doi: 10.1029/2000JA900123, 2001.

700

701 Breit, G., Tuve, M. A., A Test for the Existence of the Conducting Layer, *Phys. Rev.*, 28,
702 pp. 554-575; 1926.

703

704 Calvert, W., Cohen, R., Interpretation and Synthesis of Certain Spread-F Configurations
705 Appearing on Equatorial Ionograms, *J. Geophys. Res.*, 66 (10), 3125-32, 1961.

706

707 Candido, C. M. N., Pimenta, A. A., Bittencourt, J. A., Becker-Guedes, F., Statistical analysis
708 of the occurrence of medium-scale traveling ionospheric disturbances over Brazilian low
709 latitudes using OI 630.0 nm emission all-sky images, *Geophys. Res. Lett.*, 35, L17105, doi:
710 10.1029/2008GL035043, 2008.

711

712 Candido, C. M. N., Batista, I. S., Becker-Guedes, F., Abdu, M. A., Sobral, J. H. A.,
713 Takahashi, H., Spread F occurrence over a southern anomaly crest location in Brazil during
714 June solstice of solar minimum activity, *J. Geophys. Res.*, 116, A06316,
715 Doi:10.1029/2010JA016374, 2011.

716

717 Chapagain, N. P., Makela, J. J., Meriwether, J. W., Fisher, D. J., Buriti, R. A., Medeiros, A.
718 F., Comparison of Nighttime Zonal Neutral Winds and Equatorial Plasma Bubble Drift
719 Velocities over Brazil, *J. Geophys. Res.*, doi: 10.1029/2012JA017620, 2012.

720

721 Dao, T., Otsuka, Y., Shiokawa, K., Tulasi Ram, S., Yamamoto, M., Altitude development of
722 postmidnight F region field-aligned irregularities observed using Equatorial Atmosphere
723 Radar in Indonesia, *Geophys. Res. Lett.*, 43, 1015–1022, doi:10.1002/ 2015GL067432,
724 2016.

725

726 Fisher, D. J., Makela, J. J., Meriwether, J. W., Buriti, R. A., Benkhaldoun, Z., Kaab, M.,
727 Lagheryeb, A., Climatologies of nighttime thermospheric winds and temperatures
728 from Fabry-Perot interferometer measurements: From solar minimum to solar maximum, *J.*
729 *Geophys. Res. Space Physics*, 120, 6679–6693, doi:10.1002/2015JA021170, 2015.

730

731 Galkin, I. A., Khmyrov, G. M., Reinisch, B. W., McElroy, J., The SAOXML 5: New format
732 for ionogram-derived data, in *Radio Sounding and Plasma Physics*, AIP Conf. Proc. 974,
733 160-166, 2008.

734

735 Heisler, L. H., Anomalies in ionosonde records due to traveling ionospheric disturbances,
736 *Austr. J. Phys.*, V.11, pp. 79, 1958.

737

738 Li, G., Ning, B., Abdu, M. A., Yue, X., Liu, L., Wan, W., Hu, L., On the occurrence of
739 postmidnight equatorial F region irregularities during the June solstice, *J. Geophys. Res.*,
740 116, A04318, doi:10.1029/2010JA016056, 2011.

741

742 MacDougall, J. W., Abdu, M.A., Jayachandran, P. T., Cecile, F., Batista, I. S., Presunrise
743 spread F at Fortaleza, *J. Geophys. Res.*, 103 (A10), 23415-23425, 1998.

744

745 MacDougall, J., Abdu, M. A., Batista, I., Buriti, R., Medeiros, A. F., Jayachandran, P. T.,
746 and Borba, G., Spaced transmitter measurements of medium-scale traveling ionospheric
747 disturbances near the equator, *Geophys. Res. Lett.*, 38, L16806,
748 Doi:10.1029/2011GL048598, 2011.

749

750 Makela, J. J., Miller, E. S., Optical observations of the growth and day-to-day variability of
751 equatorial plasma bubbles, *J. Geophys. Res.*, 113, A03307, doi:10.1029/2007JA012661,
752 2008.

753

754 Makela, J. J., Miller, E. S., Tallat, E., Nighttime medium-scale traveling ionospheric
755 disturbances at low geomagnetic latitudes, *Geophys. Res. Lett.*, 37, L24104,
756 doi:10.1029/2010GL045922, 2010.

757

758 Miller, E. S., Makela, J. J., Kelley, M. C., Seeding of equatorial plasma depletions by
759 polarization electric fields from middle latitudes: Experimental evidence, *Geophys. Res.*
760 *Lett.*, 36, L18105, doi:10.1029/2009GL039695, 2009.

761

762 Munro, G. H., Heisler, L. H., Cusp-Type Anomalies in Variable Frequency Ionospheric
763 Records, *Austr. J. of Physics*, V.9 (3), 343-358, 1956.

764

765 Nicolls, M. J., Kelley, M. C., Vlasov, M. N., Sahai, Y., Chau, J. L., Hysell, D. L., Fagundes,
766 P. R., Becker-Guedes, F., Lima, W. L. C., Observations and modeling of post-midnight
767 uplifts near the magnetic equator, *Ann. Geophysicae*, 24, 1,317–1,331, 2006.

768

769 Nishioka, M., Otsuka, Y., Shiokawa, K., Tsugawa, T., Effendy, Supnithi, P., Nagatsuma, T.,
770 Murata, K. T., On post-midnight field-aligned irregularities observed with a 30.8-MHz radar at a
771 low latitude: Comparison with F-layer altitude near the geomagnetic equator, *J. Geophys. Res.*,
772 117, A08337, 732 doi:10.1029/2012JA017692, 2012.

773

774 Otsuka, Y., Ogawa, T., Effendy, VHF radar observations of nighttime F-region field-aligned
775 irregularities over Kototabang, Indonesia, *Earth Planets Space*, 61(4), 431-437, 2009.

776

777 Otsuka, Y., Review of the generation mechanisms of post-midnight irregularities in the
778 equatorial and low-latitude ionosphere, *Progress in Earth and Planetary Science*, 5:57
779 <https://doi.org/10.1186/s40645-018-0212-7>, 2017.

780

781 Paulino, I., Medeiros, A. F., Buriti, R. A., Sobral, J. H. A., Takahashi, H., Gobbi, D, Optical
782 observations of plasma bubble westward drift over Brazilian tropical region, *J. Atmos. Terr.*
783 *Phys*, V. 72 (5-6), 521-27, 2010.

784

785 Paulino, I., Medeiros, A. F., Vadas, S., Wrasse, C. M., Takahashi, H., Buriti, R. A., Leite,
786 D., Figueira, S., Bageston, J. V., Sobral, J.H.A., Gobbi, D., Periodic waves in the lower
787 thermosphere observed by OI630nm airglow images. *Ann. Geophys.*, 34, 293–301, 2016.

788

789 Pimenta, A. A., Amorim, D., Candido, C. M. N., Thermospheric dark band structures at low
790 latitudes in the Southern Hemisphere under different solar activity conditions: A study using
791 OI 630 nm emission all-sky images, *Geophys. Res. Lett.*, 35, p. L16103,
792 doi:10.1029/2008GL034904, 2008.

793

794 Ratcliffe, J. A., Some Irregularities in the F2 Region of the Ionosphere, *J. Geophys. Res.*,
795 50(4), 487-507, 1956.

796

797 Reinisch, B. W., Abdu, M. A., Batista, I. S., Sales, G. S., Khmyrov, G., Bullett, T. A., Chau,
798 T., Rios, V., Multistation digisonde observations of equatorial spread F in South America,
799 *Ann. Geophys.*, 22, 3145–3153, 2004.

800

801 Reinisch, B. W., Huang, X., Galkin, I. A., Paznukhov, V., Kozlov, A., Recent advances in
802 the real-time analysis of ionograms and ionospheric drift measurements with digisondes, J.
803 Atmos. Terr. Phys., 67 (2005) 1054–1062, 2005.

804

805 Sahai, Y., Fagundes, P. R., Bittencourt, J. A., Transequatorial F-region ionospheric plasma
806 bubbles solar cycle effects, Journal of Atmospheric and Solar-Terrestrial Physics, 62: 1377-
807 1383, 2000.

808

809 Sobral, J. H. A., Abdu, M. A.; Takahashi, H., Taylor, M. J., de Paula, E. R., Zamlutti, C. J.,
810 Aquino, M. G.; Borba, G. L., Ionospheric plasma bubble climatology over Brazil based on
811 22 years (1977-1998) of 630 nm airglow observations, Journal of Atmospheric and Solar-
812 Terrestrial Physics, 64: 1517-1524, 2002.

813

814 Sobral, J. H. A., deCastilho, V. M., Abdu, M. A., Takahashi, H., Paulino, I, Gasparelo, U. A.
815 C., Arruda, D. C. S., Mascarenhas, M., Zamlutti, C. J., Denardini, C. M., Koga, D.,
816 deMedeiros, A. F., Buriti, R. A., Midnight reversal of ionospheric plasma bubble eastward
817 velocity to westward velocity during geomagnetically quiet time: Climatology and its model
818 validation, J. Atmos. Terr. Phys., 73, 1520–1528, 2011.

819

820 Takahashi, H., Wrasse, C. M., Figueiredo, C. A. O. B., Barros, D., Abdu, M.A., Otsuka, Y.,
821 Shiokawa, K., Equatorial plasma bubble seeding by MSTIDs in the ionosphere, Progress in
822 Earth and Planetary Science, 5:32, 2018.

823

824 Valladares, C. E., Hanson, W. B., McClure, J. P., Cragin, B .L., Bottomside sinusoidal
825 irregularities in the equatorial F region, *Journal of Atm. and Solar-Terr Phys*, V. 88 (A10),
826 <https://doi.org/10.1029/JA088iA10p08025>, 1983.

827

828 Yizengaw, E., Retterer, J., Pacheco, E. E., Roddy, P., Groves, K., Caton, R., Baki, P.,
829 Postmidnight bubbles and scintillations in the quiet-time June solstice, *Geophys. Res. Lett.*,
830 40, doi:10.1002/2013GL058307, 2013.

831

832 Yokoyama, T., Yamamoto, M., Otsuka, Y., Nishioka, M., Tsugawa, T., Watanabe, S. and
833 Pfaff, R. F., On post-midnight low latitude ionospheric irregularities during solar minimum:
834 1. Equatorial Atmosphere Radar and GPS TEC observations in Indonesia, *J. Geophys. Res.*,
835 116, A11325, doi:10.1029/2011JA016797, 2011.

836

837 Zhan, W., Rodrigues, F., Milla, M., On the genesis of postmidnight equatorial spread *F*:
838 Results for the American/Peruvian sector, *Geophysical Research Letters*, 45, 7354–7361.
839 <https://doi.org/10.1029/2018GL078822>, 2018.

840

841

842

843

844

845

846

847

848

849

850

851

852

853

854

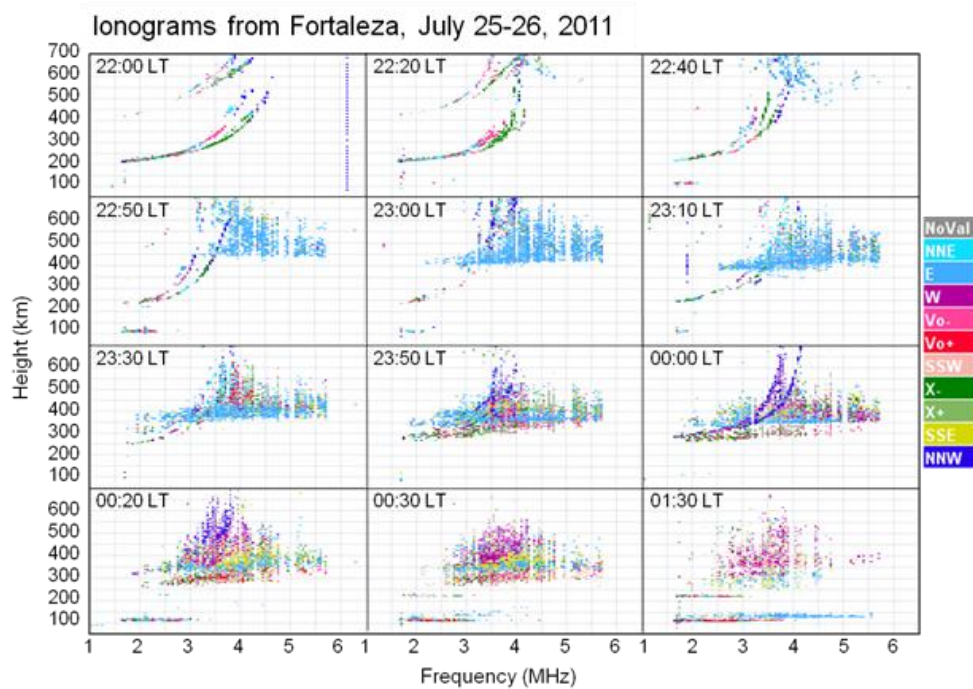
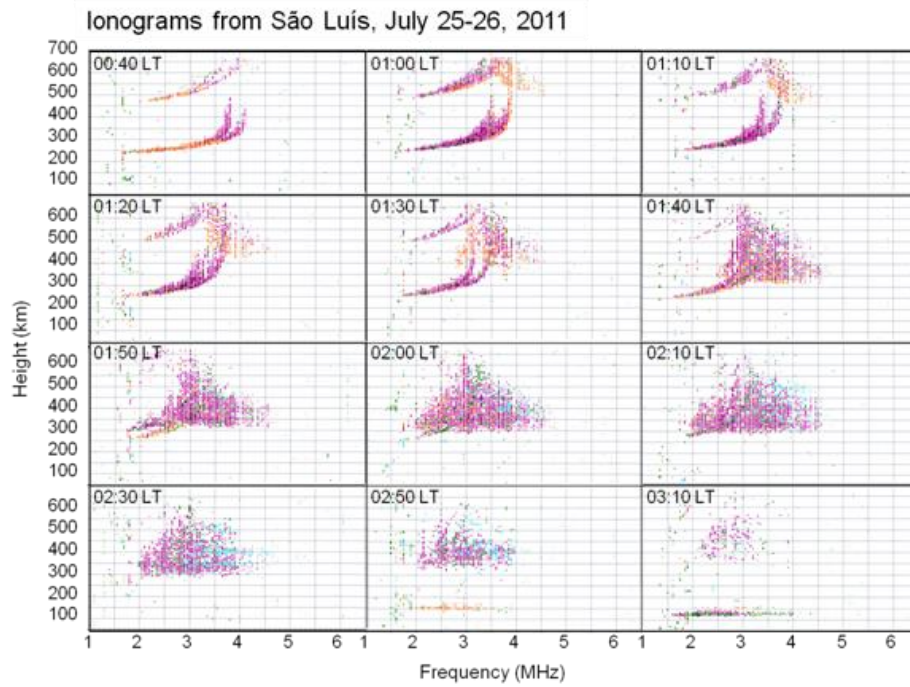
855

856

857

858

859 Figure 1

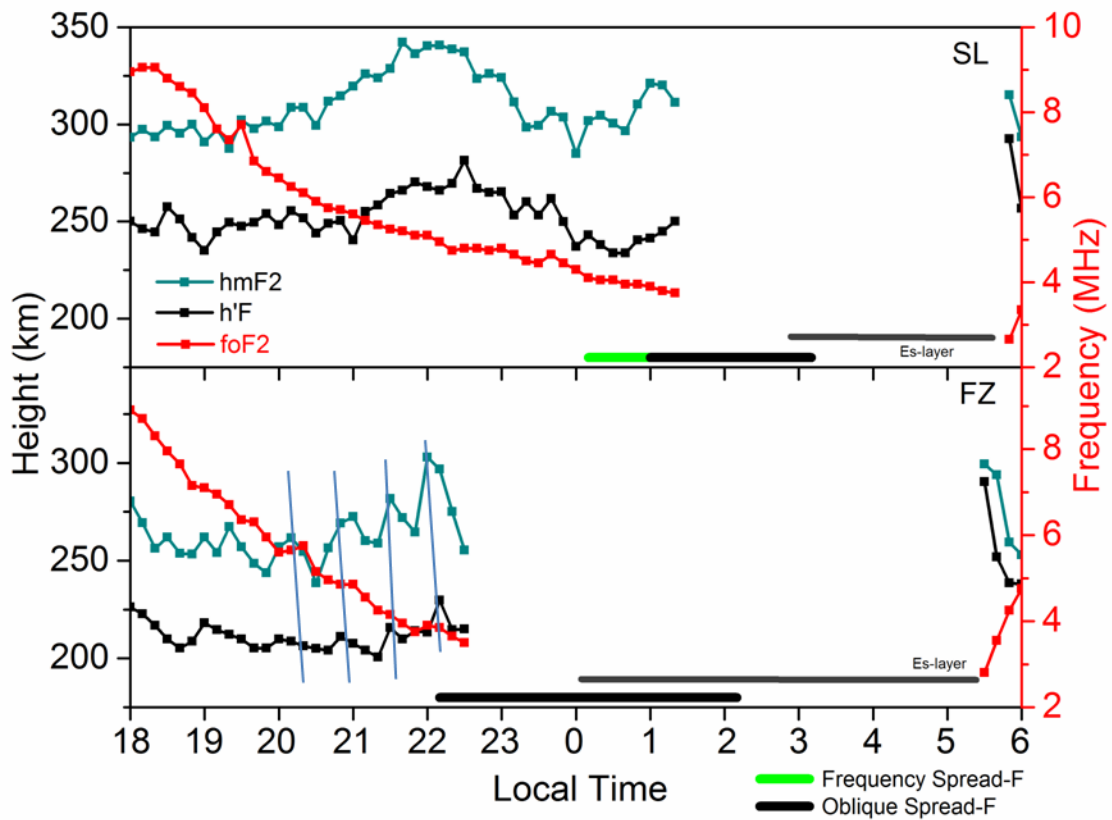


860

861

862 **Figure 1:** Sequence of ionograms obtained on July 25-26, at São Luis, from 00:40 to 03:10
 863 LT and over FZ, Brazil, 2011, from 22:00 to 01:30 LT. The spread-F shows an unusual
 864 pattern, with oblique echoes. The color scale in FZ ionograms indicates echoes are coming
 865 from the east and propagating to the westward.

866 Figure 2



867

868 **Figure 2:** F-layer parameters $h'F$ (km), $hmF2$ (km) and $foF2$ (MHz), on July 25-26, 2011

869 obtained from the Digisondes at **SL (top panel) and FZ (bottom panel).**

870

871

872

873

874

875

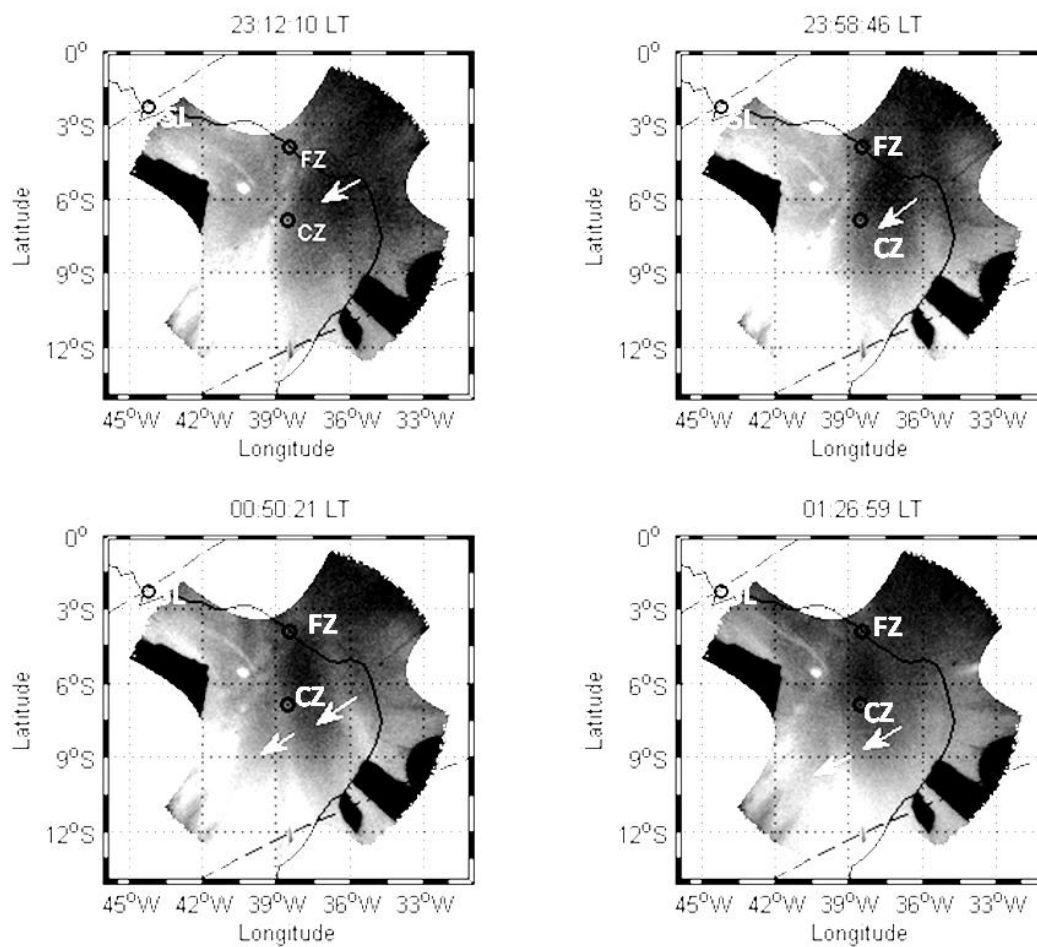
876

877

878

879 Figure 3

Images of the OI 630-nm emission from Cajazeiras July 25-26, 2011



881

882 **Figure 3:** Sequence of OI 630-nm images showing the time evolution of depletions on July
 883 25-26, 2011, between 23:12 LT and 01:26 LT at Cajazeiras, Brazil. The images are
 884 projected onto geographic coordinates over the Brazil map. In the plot, FZ is Fortaleza, SL
 885 is Sao Luis, and CZ is Cajazeiras. Arrows indicate the propagation direction of the
 886 depletions (dark regions passing over FZ and CZ)

887

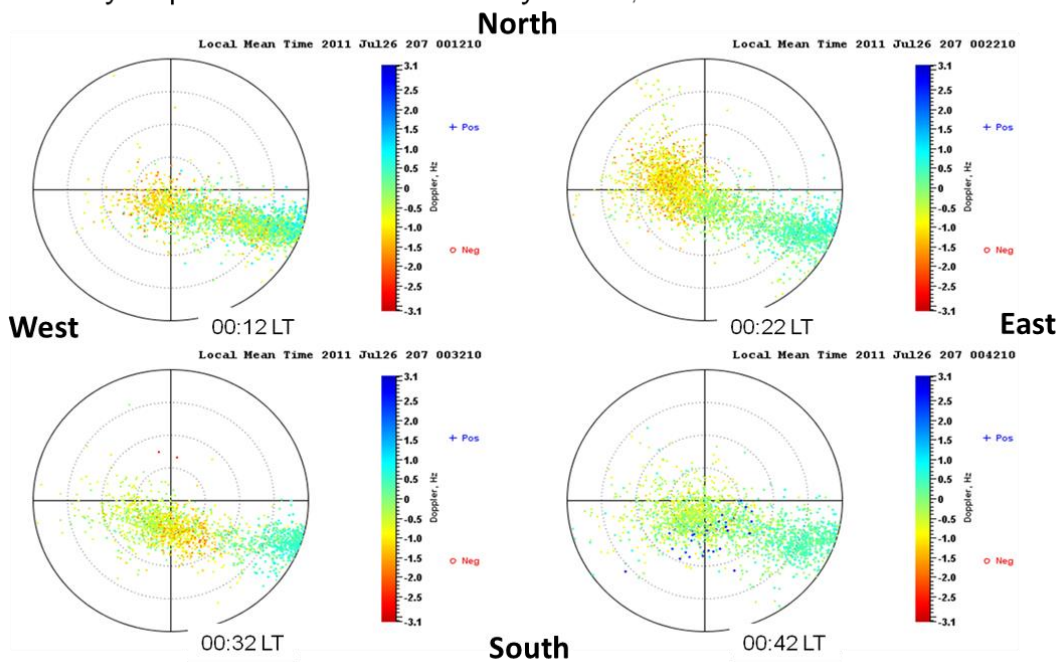
888

889

890

891 Figure 4

Skymaps from Fortaleza on July 25-26, 2011



892

893

Figure 4: Skymaps registered over FZ from 00:12 LT to 00:42 LT on July 26, 2011, showing the echoes location and Doppler frequencies (color-coded) for F-region echoes from Digisondes. Doppler velocities: Positive: irregularities arriving at the station; Negative: irregularities leaving the station.

897

898

899

900

901

902

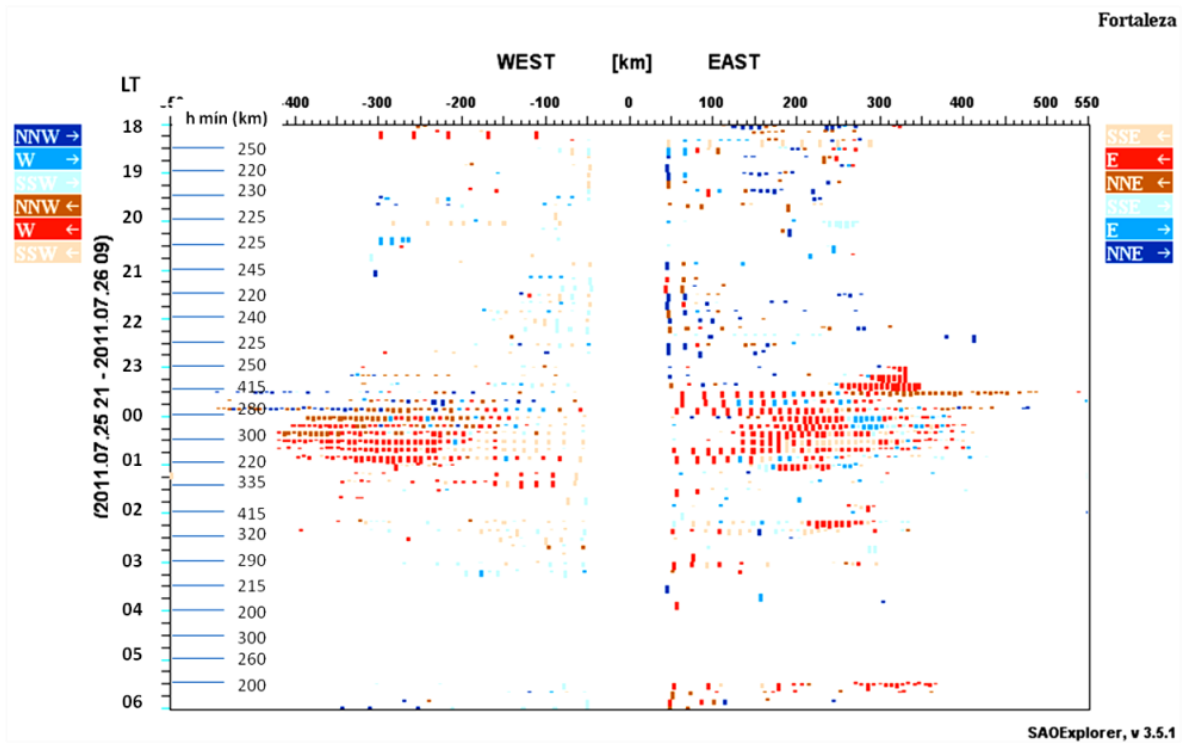
903

904

905

906

907 Figure 5



908

909 **Figure 5:** Directogram for Fortaleza on July 26 showing the location and the horizontal
 910 distances of the irregularities detected by Digisonde and seen in the ionograms as spread-F.
 911 At left: F-region height (km), where hmin is spread-F reflection height. Color code with
 912 arrows indicates the direction where the irregularities are coming from or where the
 913 irregularities are moving to.

914

915

916

917

918

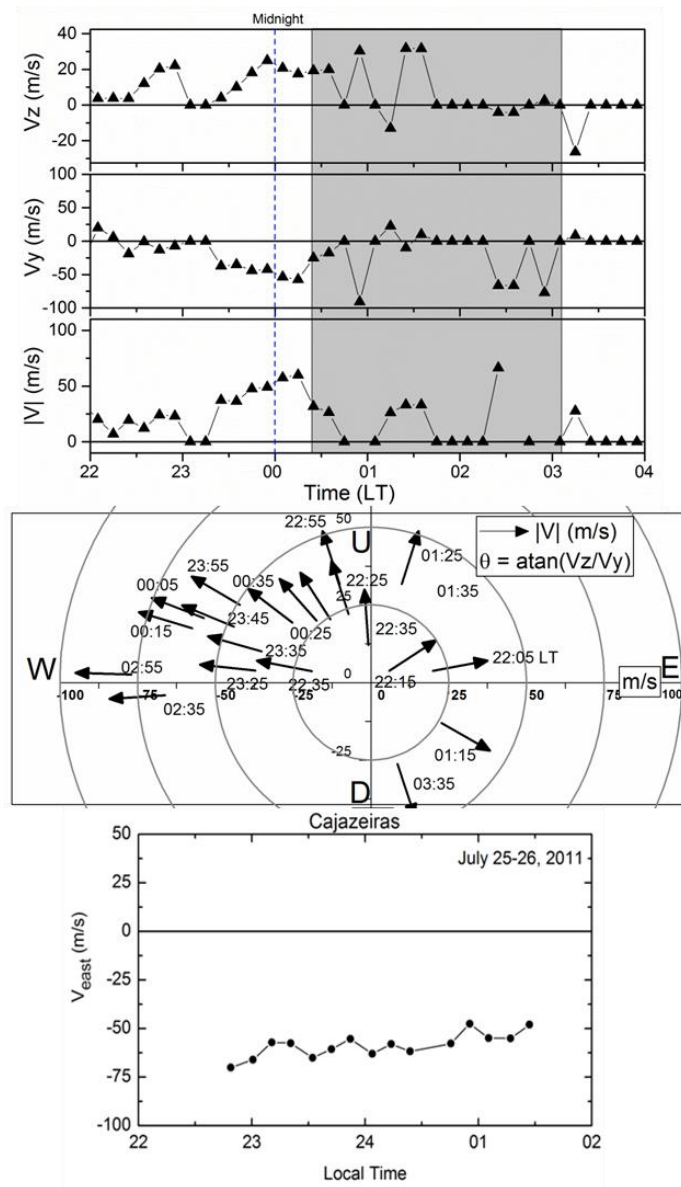
919

920

921

922

923 Figure 6

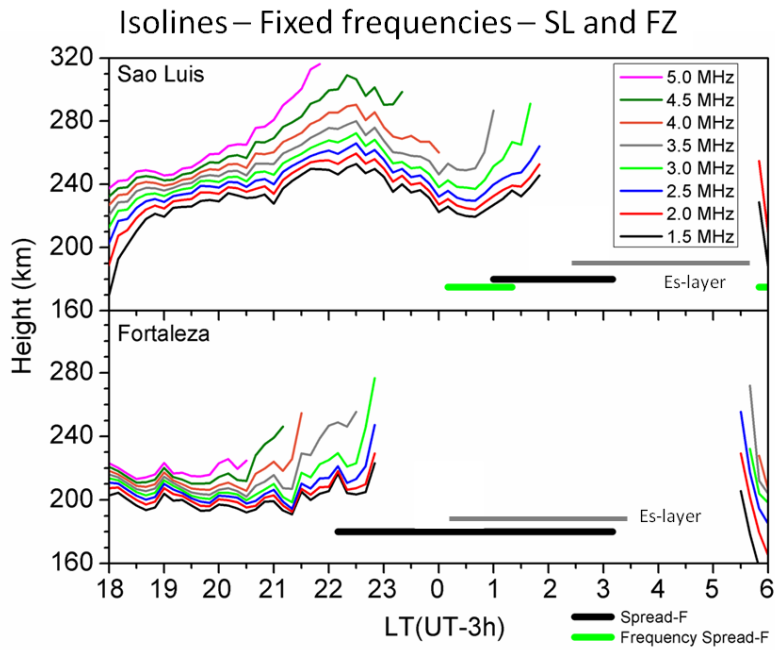


925

926 Figure 6: Top Panel: Vertical (V_z) and zonal drift (V_y) velocities on July 25-26, 2011 over
 927 FZ from 22:00 LT to 04:00 LT. $V_{\text{east}} > 0$. Middle Panel: Vector diagram showing the
 928 variations and directions of the mean total drift velocity of the irregularities seen as spread-F
 929 in ionograms. For clarity, the $|V|$ values are represented by the arrow start points. Bottom
 930 panel: Zonal drift velocities obtained from the depletions seen on the OI 630.0 nm emission
 931 images obtained at CZ on July 25-26, 2011 for comparison.

932

933 Figure 7



934

935 Figure 7: Oscillations in the real height of F-layer, at fixed frequencies (1.5 to 5.0 MHz)

936 prior the spread-F in São Luis (top panel) and Fortaleza (bottom panel).

937

938

939

940

941

942

943

944

945

946

947

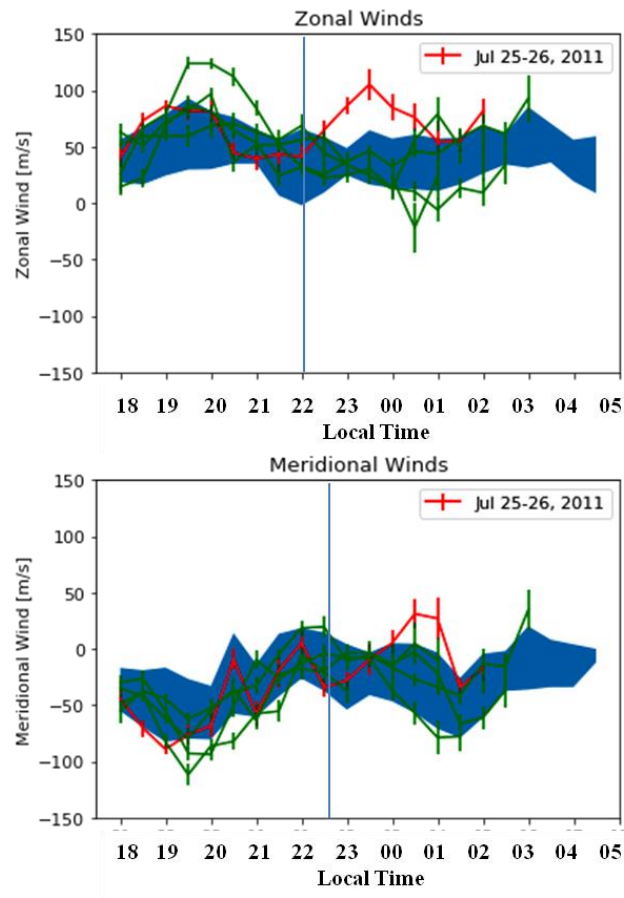
948

949

950

951 Figure 8

952



953

954 Figure 8: Measured Zonal and Meridional Winds in CZ, Brazil, in July 2011. The shaded
955 region is the **monthly average with standard deviation**, the green lines are the mean winds on
956 July 25-26 (mean of 2 days), and the red line is for July 25-26.

957

958

959

960

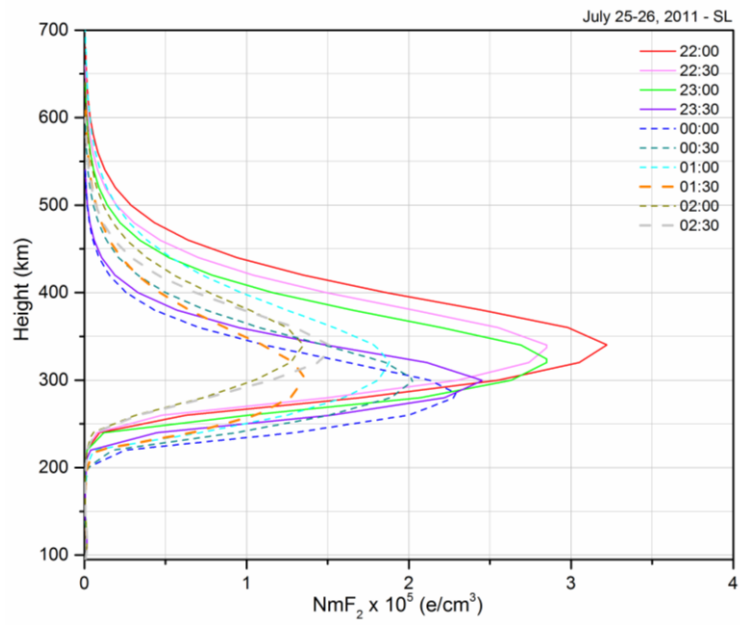
961

962

963

964 Figure 9

965



966

967 Figure 9: F-layer plasma density profile for July 25-26. derived from Digisonde data and
968 SAO Explorer data .

969

970

971

972

973

974

975

976

977

978

979

980

981 **List of figures**

982

983 Figure 1: Sequence of ionograms obtained on July 25-26, at São Luis, from 00:40 to 03:10
984 LT and over FZ, Brazil, 2011, from 22:00 to 01:30 LT. The spread-F shows an unusual
985 pattern, with oblique echoes. The color scale in FZ ionograms indicates echoes are coming
986 from the east and propagating to the westward.

987

988 **Figure 2:** F-layer parameters $h'F$ (km), $hmF2$ (km) and $foF2$ (MHz), on July 25-26, 2011
989 obtained from the Digisondes at **SL (top panel) and FZ (bottom panel).**

990

991 **Figure 3:** Sequence of OI 630-nm images showing the time evolution of depletions on July
992 25-26, 2011, between 23:12 LT and 01:26 LT at Cajazeiras, Brazil. The images are
993 projected onto geographic coordinates over the Brazil map. In the plot, FZ is Fortaleza, SL
994 is Sao Luis, and CZ is Cajazeiras. Arrows indicate the propagation direction of the
995 depletions **(dark regions passing over FZ and CZ)**

996

997 Figure 4: Skymaps registered over FZ from 00:12 LT to 00:42 LT on July 26, 2011,
998 showing the echoes location and Doppler frequencies (color-coded) for F-region echoes
999 from Digisondes. Doppler velocities: Positive: irregularities arriving at the station; Negative:
1000 irregularities leaving the station.

1001

1002 **Figure 5:** Directogram for Fortaleza on July 26 showing the location and the horizontal
1003 distances of the irregularities detected by Digisonde and seen in the ionograms as spread-F.
1004 At left: F-region height (km), where h_{min} is spread-F reflection height. **Color code with**
1005 **arrows indicates the direction where the irregularities are coming from or where the**
1006 **irregularities are moving to.**

1007

1008 Figure 6: Top Panel: Vertical (V_z) and zonal drift (V_y) velocities on July 25-26, 2011 over
1009 FZ from 22:00 LT to 04:00 LT. $V_{\text{east}} > 0$. Middle Panel: Vector diagram showing the
1010 variations and directions of the mean total drift velocity of the irregularities seen as spread-F
1011 in ionograms. Bottom Panel: Zonal drift velocities obtained from the depletions seen on the
1012 OI 630.0 nm emission images obtained at CZ on July 25-26, 2011.

1013

1014 Figure 7: Oscillations in the real height of F-layer, at fixed frequencies (1.5 to 5.0 MHz)
1015 prior the spread-F in São Luis (top panel) and Fortaleza (bottom panel).

1016

1017 Figure 8: Measured Zonal and Meridional Winds in CZ, Brazil, in July 2011. The shaded
1018 region is the monthly average with standard deviation, the green lines are the mean winds on
1019 July 25-26 (mean of 2 days), and the red line is for July 25-26.

1020

1021 Figure 9: F-layer plasma density profile for July 25-26. derived from Digisonde data and
1022 SAO Explorer data

1023

1024

1025

1026

1027

1028

1029

1030

1031